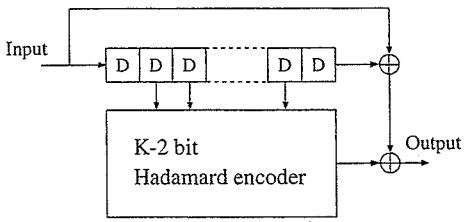

Figure 1. Encoder for SOCC of arbitrary constraint length K.

2.1. THE SUPER-ORTHOGONAL CONVOLUTIONAL CODES

Before describing the overall system model, it is useful to provide the encoder structure of SOCC and its important properties. The SOCC is a family of very low-rate orthogonal convolutional codes (VLORCC) proposed by Viterbi [1]. Figure 1 shows the SOCC encoder. The encoder has a shift register of length K and block orthogonal (Walsh-Hadamard) encoder. First, let us define the Walsh-Hadamard matrix as

$$\mathbf{H}_k = \begin{pmatrix} \mathbf{H}_{k-1} & \mathbf{H}_{k-1} \\ \mathbf{H}_{k-1} & \overline{\mathbf{H}}_{k-1} \end{pmatrix}, \quad \mathbf{H}_0 = 0, \tag{1}$$

where k is a nonzero integer, and $\overline{\mathbf{H}}_k$ is the complement of $\mathbf{H}_k$. In the K bit shift register, the inner $(K-2)$ bit memories are mapped into one Walsh sequence of length 2^{K-2}. Then, the remaining two outer bits are added to the selected Walsh sequence by modulo-2 addition. The resultant code rate is given by $R_c = 2^{-K+2}$.

The decoding is performed by using Viterbi algorithm (VA). In the trellis diagram of SOCC, there are two branches emanating from each state corresponding to two different bits. There are also two branches merging into each state. The mapping rule, adding the two outer memories to the selected Walsh sequence, guarantees that in the trellis diagram any two output sequences leaving and entering each state are complementary to each other. This effectively increases the minimum free distance of the codes compared to the previously proposed orthogonal and bi-orthogonal convolutional codes [1].

It should also be noted that as K increases the performance of SOCC is improved, approaching the Shannon capacity as $K \to \infty$. In addition to their near optimum performance, the SOCC has an additional advantage that the decoder structure is relatively simple because decoding is performed based on VA.

2.2. TRANSMIT SIGNAL MODEL

The overall system model considered is shown in Figure 2. At the transmitter, a binary information stream $\boldsymbol{d}_k \triangleq \left(d_0^k, d_1^k, \ldots, d_{N_b-1}^k\right)$ is encoded by a SOCC encoder of coding rate $R_c = 1/L_c$, where k and N_b denote the user number and the number of transmitted bits. The resultant stream of binary codewords are converted to antipodal signal stream $\boldsymbol{b}_k \triangleq \left(b_0^k, b_1^k, \ldots, b_{L_c N_b-1}^k\right)$, which is then spread by a user-specific spreading sequence. The

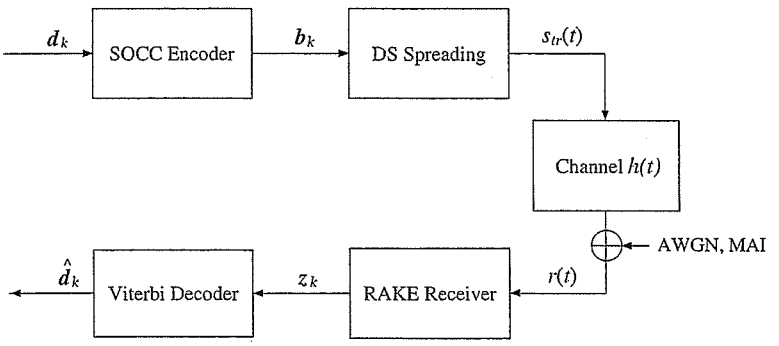

Figure 2. The overall system model of DS-UWB.

baseband transmit signal for the kth user is given by

$$s_{tr}^k(t) = \sum_{n=0}^{L_c N_b - 1} b_n^k p_n^k(t - nT_s), \tag{2}$$

where T_s denotes the symbol duration, and $p_n^k(t)$ is a signature waveform of duration T_s defined as

$$p_n^k(t) = \sqrt{\frac{E_s}{N_c}} \sum_{i=0}^{N_c - 1} c_i^k(n)\rho(t - nT_c), \tag{3}$$

where E_s denotes the symbol energy. The transmit pulse shape $\rho(t)$ is a Gaussian waveform of duration T_p, whose energy is normalized as $\int_0^{T_p} |\rho(t)|^2 dt = 1$. The pulse width is assumed to be less than the chip duration T_c, i.e., $T_p < T_c$. For simplicity, we assume $T_s = N_c T_c$. Let

$$\boldsymbol{c}^k(n) \triangleq \left[c_0^k(n), c_1^k(n), \ldots, c_{N_c-1}^k(n)\right]^T \tag{4}$$

denote a pseudo-random spreading sequence of length N_c, where $(\cdot)^T$ denotes transpose operation. The spreading sequence assumes the value of $\{\pm 1\}$ (DS spreading).

In this case, the total spreading factor can be represented as the product of two kinds of bandwidth expansion factor, i.e., $N = F_s F_c$, where $F_s = N_c$ and $F_c = 1/R_c$. The first term is the bandwidth expansion factor by spreading, and the second one is the bandwidth expansion factor by channel coding, and the two types of bandwidth expansion factors are freely interchangeable. Thus, the use of low-rate codes, under the constraint that the total spreading factor N is fixed, clearly, shortens the length of spreading sequence, which leads to poor correlation characteristics of the spreading sequences. In addition to this, it is well known that the correlation characteristics of the Walsh sequences, which are used as codewords of SOCC, are poor. This means that the SO coded UWB system suffers severely from MUI as well as ISI by considering that in typical UWB channel there exists hundreds of multipath having large delay-spread and many uncooperative UWB devices in other piconets.

In order to reduce the effect of ISI and MUI, the use of several spreading sequences per single user, which throughout of this paper is referred to as *code-hopping*, is proposed. In the code-hopping (CH) scheme, spreading sequences are switched between a predetermined set of sequences. This results in different interferences from symbol to symbol and makes the

interference probability density function (pdf) closely approximate the Gaussian distribution. We define the number of pre-determined sequence per single user as J. Let

$$\boldsymbol{a}^k = \left[\boldsymbol{a}^k(0), \boldsymbol{a}^k(1), \ldots, \boldsymbol{a}^k(J-1)\right] \tag{5}$$

be a set of sequences allocated for the kth user, where

$$\boldsymbol{a}^k(j) = \left[a_0^k(j), a_1^k(j), \ldots, a_{N_c-1}^k(j)\right]^T \in \{\pm 1\} \tag{6}$$

for $0 \leq j < J$. Then, the sequences are switched from symbol to symbol so that

$$\boldsymbol{c}^k(n) = \boldsymbol{a}^k(n \bmod J). \tag{7}$$

2.3. Received Signal Model

The signal $s_{\mathrm{tr}}(t)$ is transmitted through a channel having impulse response $h_k(t)$ written as [8]

$$h_k(t) = \sum_{l=1}^{L_{\max}} \alpha_l^k \delta(t - \tau_l^k), \tag{8}$$

where $L_{\max}$ is the number of multipath components, α_l^k and τ_l^k denote, respectively, the received amplitude and the delay of the lth path. The total energy of $h_k(t)$ is normalized, i.e., $\int_0^{T_{\max}} |h_k(t)|^2 dt = 1$, where $T_{\max}$ denotes the maximum delay spread.

Defining $\tilde{p}_n^k(t) = h_k(t) * p_n^k(t)$ as the received signature waveform, the received signal may be written as

$$\begin{aligned} s_{\mathrm{rec}}^k(t) &= \sum_{n=0}^{N_b-1} b_n^k \tilde{p}_n^k(t - nT_s) \\ &= \sum_{n=0}^{N_b-1} b_n^k \sum_{l=1}^{L_{\max}} \alpha_l^k \rho(t - nT_s - \tau_l). \end{aligned} \tag{9}$$

Assume that N_u transmitters are active, then the total received signal is represented as follows.

$$r(t) = \sum_{k=1}^{N_u} A_k s_{\mathrm{rec}}^k(t - \tau_k) + \nu(t), \tag{10}$$

in which A_k and τ_k are the channel attenuation and relative time offset between transmitted signal of the kth user and receiver of the desired user. Without loss of generality, assume the desired user as user 1. The AWGN with two-sided power spectral density $N_0/2$ is denoted by $\nu(t)$.

2.4. RAKE Receiver Structure

In this paper, a coherent RAKE receiver followed by matched filter (MF) is considered to exploit the multipath diversity and combat the fading inherent to realistic channels. Since in UWB channel there exists hundreds of multipath components, it is too expensive in terms of

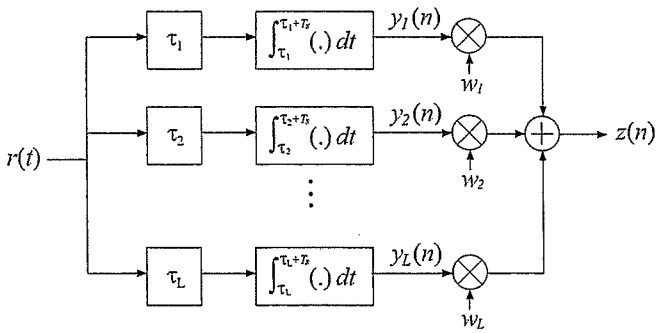

Figure 3. L-branch coherent RAKE receiver.

complexity to gather them all. Thus, we adopt a suboptimum method where only the largest L out of $L_{\max}$ paths are combined, called selective RAKE (S-RAKE) in the literature [11].

Let $\{\lambda_l\}_{l=1}^{L}$ and $\{\theta_l\}_{l=1}^{L}$ denote the estimation of the amplitude and delay, respectively, of the selected largest L paths. The subscript l is ordered by the delay time (i.e., $\theta_1 < \theta_2 < \cdots < \theta_L$). In order to make theoretical analysis tractable, the following assumptions are made. First, the synchronization between transmitter and receiver for desired user is perfectly established, i.e, $\tau_1 = 0$. Secondly, the receiver of the desired user can perfectly estimate the channel response $h_1(t)$ prior to data transmission by using some pilot symbols. Finally, the signature waveforms for all users have the same period, while the desired user's receiver does not know the timing offset τ_k or the channel response $h_k(t)$ for other interference users ($2 \leq k \leq N_u$). This assumption is valid considering that the typical UWB assumes peer-to-peer transmission.

Figure 3 shows the RAKE receiver structure considered in this paper. As shown in Figure 3, the receiver consists of a bank of L RAKE fingers, each correlating to a different delay of the received signal. Without loss of generality, we consider the nth symbol. Let $\boldsymbol{y}(n)$ denote the MF output given by

$$\boldsymbol{y}(n) = [y_1(n), y_2(n), \ldots, y_L(n)]^T , \tag{11}$$

whose elements denote the MF outputs corresponding to each path.

$$y_l(n) = \int_{\theta_l}^{\theta_l + T_s} r(t + nT_s) \cdot p_n^1(t - \theta_l) dt \tag{12}$$

for $0 \leq l < L$. The MF outputs are then combined to form a decision statistics. Let us define the combining weight for the coherent RAKE receiver as

$$\boldsymbol{w}(n) = [w_1(n), w_2(n), \ldots, w_L(n)]^T . \tag{13}$$

Note that the combining weight is a function of symbol index n when CH is employed since the received vector is changed from symbol to symbol. The derivation of the combining weight is shown in the next section. The decision statistic corresponding to the nth symbol is given by

$$z(n) = \boldsymbol{w}^T(n)\boldsymbol{y}(n). \tag{14}$$

By using the decision variable in (14), the decoding metric is calculated and decoding is performed by VA.

3. Performance Analysis

In this paper, two types of RAKE combining schemes, MRC combining and MMSE combining receivers, are considered. It is known that MRC is optimum under the AWGN channel, however it is not under other channels. On the contrary, MMSE combining receiver has the capability to effectively suppress the interferences such as ISI and MUI. In this section, the derivation of the combining weight for MRC and MMSE combining are, respectively, presented. Following, the upper bound of average BER is derived.

3.1. Derivation of the Combining Weight

Since the correlator output is composed of the sum of the signal components from all users, the MF outputs in (11) can be written as

$$y(n) = \sum_{k=1}^{N_u} \boldsymbol{G}_k(n)\boldsymbol{b}_k(n) + \tilde{\boldsymbol{v}}(n), \tag{15}$$

where, the vector of length N_a $\boldsymbol{b}_k(n) = [b_0^k(n), \ldots, b_{N_a-1}^k(n)]^T \in \{\pm 1\}$ denotes the polarity of the kth user's signal, $\tilde{\boldsymbol{v}}(n) = \left[\tilde{v_1}(n), \tilde{v_2}(n), \ldots, \tilde{v_L}(n)\right]$ represents the noise term after despreading as

$$\tilde{v_l}(n) = \int_{\theta_l}^{\theta_l+T_s} v(t + nT_s)p_n^1(t - \theta_l)dt. \tag{16}$$

In (15), L-by-N_a matrix $\boldsymbol{G}_k(n)$ represents interference coefficients, where N_a is the maximum number of symbols in an observation time $T_w = \theta_L - \theta_1 + T_s$. In more details, N_a can be expressed as $N_a = N_l + N_r$, where $N_l = \lceil T_{max}/T_s \rceil$, $N_r = \lceil T_w/T_s \rceil$. The coefficient matrix $\boldsymbol{G}_k(n)$ is expressed as

$$\boldsymbol{G}_k(n) = \left[\boldsymbol{g}_1^k(n), \ldots, \boldsymbol{g}_{N_a}^k(n)\right]. \tag{17}$$

Each column vector

$$\boldsymbol{g}_i^k(n) = \left[g_{i,1}^k(n), \ldots, g_{i,L}^k(n)\right]^T \tag{18}$$

represents the interference coefficient from the ith symbol of the kth user. Note that $\boldsymbol{g}_{N_l}^1(n)$ represents the desired output. Each element of $\boldsymbol{g}_i^k(n)$ is expressed as

$$g_{i,l}^k(n) = \sum_{m=1}^{L_{max}} \alpha_m^k f_{1,k}\left(\tau_m^k + \tau_k + (i - N_l)T_s - \theta_l\right), \tag{19}$$

where $f_{1,k}(x)$ denotes the aperiodic cross-correlation function between $p_{1,n}(t)$ and $p_{k,i}(t)$

$$f_{1,k}(x) = \int_0^{T_s} p_{1,n}(t)p_{k,i}(t + x)dt. \tag{20}$$

Here, because of the independence assumption on the AWGN components as well as the interference from different users of different RAKE branches, the correlation matrix of MF outputs

(15) is expressed as follows.

$$\begin{aligned}\boldsymbol{R}(n) &= \mathrm{E}\left[\boldsymbol{y}(n)\boldsymbol{y}^T(n)\right] \\ &= \sum_{k=1}^{N_u} \boldsymbol{G}_k(n)\boldsymbol{G}_k^T(n) + \sigma_n^2 \boldsymbol{I}_L, \end{aligned} \tag{21}$$

where, $\mathrm{E}[\cdot]$ and $\boldsymbol{I}_L$ denote the mathematical expectation and a L-by-L identity matrix. Based on the MMSE criterion, the optimum filter weight for MMSE combining case converges into the following solution.

$$\begin{aligned}\boldsymbol{w}_{\mathrm{MMSE}}(n) &= \arg\min_{\boldsymbol{w}} \mathrm{E}\left[\left(\boldsymbol{w}^T(n)\boldsymbol{y}_l(n) - d_n^1\right)^2\right] \\ &= \boldsymbol{R}^{-1}(n)\boldsymbol{p}(n), \end{aligned} \tag{22}$$

where $\boldsymbol{p}(n)$ is given by

$$\begin{aligned}\boldsymbol{p}(n) &= \mathrm{E}\left[\boldsymbol{y}(n)d_1(n)\right] \\ &= \boldsymbol{g}_{1,N_l}(n). \end{aligned} \tag{23}$$

When short code spreading is employed (i.e., $J = 1$), the correlation matrix and the steering vector do not depend on n, i.e., $\boldsymbol{R}(n) = \boldsymbol{R}$, $\boldsymbol{p}(n) = \boldsymbol{p}$. Accordingly, the combining weight is uniqely determined as $\boldsymbol{w}_{\mathrm{MMSE}}(n) = \boldsymbol{w}_{\mathrm{MMSE}}$. However, in the case of CH ($J \geq 2$), since J kinds of sequences are used, the calculation of $\boldsymbol{R}(j)$ and $\boldsymbol{w}(j)$ for $0 \leq j < J$ must be effectuated. In the case of MRC combining receiver, the weight is simply obtained as

$$\boldsymbol{w}_{\mathrm{MRC}}(n) = \boldsymbol{\lambda}, \tag{24}$$

where $\boldsymbol{\lambda} = [\lambda_1, \ldots, \lambda_L]^T$.

3.2. Derivation of Signal-to-Interface Plus Noise Ratio

Signal-to-interference plus noise ratio (SINR) is derived in order to obtain the BER expression. In this paper, in order to simplify the analysis, MUI and ISI are both assumed to be Gaussian distribution (Gaussian approximation). By using the weight derived in the (22) and (24), the SINR per symbol at the output of the RAKE receiver for both MRC and MMSE combining can easily written as

$$\gamma_n = \frac{\boldsymbol{w}^T(n)\boldsymbol{R}_s(n)\boldsymbol{w}(n)}{\boldsymbol{w}^T(n)\boldsymbol{R}_I(n)\boldsymbol{w}(n)}, \tag{25}$$

where $\boldsymbol{R}_s$ and $\boldsymbol{R}_I$ denote the correlation matrix for the desired output and for the total interference including ISI, MUI, and AWGN, given by

$$\boldsymbol{R}_s(n) = \boldsymbol{g}_{1,N_l}(n)\boldsymbol{g}_{1,N_l}^T(n) \tag{26}$$

$$\boldsymbol{R}_I(n) = \boldsymbol{R}(n) - \boldsymbol{R}_s(n). \tag{27}$$

When using multiple spreading sequence, each SINR is averaged as

$$\bar{\gamma} = \frac{1}{J}\sum_{j=0}^{J-1}\gamma_j. \tag{28}$$

3.3. Upper Bound of Bit Error Rate

The upper bound of the BER of any convolutional codes can be obtained from the generating function $T(X, Y)$. The union bound of the BER is given by [12]

$$P_b < \frac{1}{k}\frac{dT(X,Y)}{dY}\Big|_{Y=1} \tag{29}$$

$$= \frac{1}{k}\sum_{d=d_f}^{\infty} B_d X^d, \tag{30}$$

where $X = \exp(-\bar{\gamma})$. Here the SINR derived in (25) is a function of α_l^k and τ_l^k for $1 \le k \le N_u$, $1 \le l \le L$. Because SV model is not a stochastic model, it is difficult to obtain an exact solution of average bit error probability. Thus, it is numerically calculated.

4. Numerical Results

In this section, the bit error performance of SO coded scheme is compared with the other convolutional coded scheme based on computer simulations.

4.1. Simulation Parameters

Table 1 shows the parameters applied for convolutional codes (CC) and spreading sequences. As shown in this table, three types of convolutional codes, that is, CC of coding rate 1/2 (denoted as CC 1 in Table 1) and CC of coding rate 1/4 (denoted as CC 2 in Table 1), as well as SOCC, are considered. For each code, two different constraint lengths, $K = 5$ and 6, are considered. Note that for SOCC, coding rate is given by 1/8 and 1/16 for $K = 5$ and 6, respectively, from the relationship between the constraint length and the coding rate. In order to make a fair comparison, all codes have the same number of states in trellis diagram (or equivalently, the same memory size at the encoder). At the decoder, soft-decision Viterbi decoding is assumed for each scheme. As for the spreading sequence, Gold sequences of length N_c are employed. The length of Gold sequences are set so that the total bandwidth expansion factor $N = N_c/R_c$ is almost the same ($N \simeq 255$ in this case) for all schemes. The number of RAKE fingers is fixed to $L = 8$ for all schemes. The pulse duration and the chip duration are both 2.0 ns. The data transmission rate is given by $R_b = 1/(NT_c)$. Because of the size limitation, only the result for channel model (CM) 3 is shown. Since CM 3 has relatively large number of paths and delay-spread, the performance degradation due to ISI and MUI can be easily observed. Although $L = 8$ is employed in this paper, the bigger the values given to L are, the more significant the performance improvement becomes. This is the trade-off between performance improvement and implementation complexity.

Table 1. Coding and spreading parameters

Scheme	Constraint length (K)	Coding rate (R_c)	Generating function	Sequence length (N_c)	Total spreading factor (N)
CC1	5	1/2	$[23, 35]_8$	127	254
	6	1/2	$[53, 75]_8$	127	254
CC2	5	1/4	$[25, 27, 33, 37]_8$	63	252
	6	1/4	$[53, 67, 71, 75]_8$	63	252
SOCC	5	1/8	–	31	248
	6	1/16	–	15	240
Uncoded	–	1	–	255	255

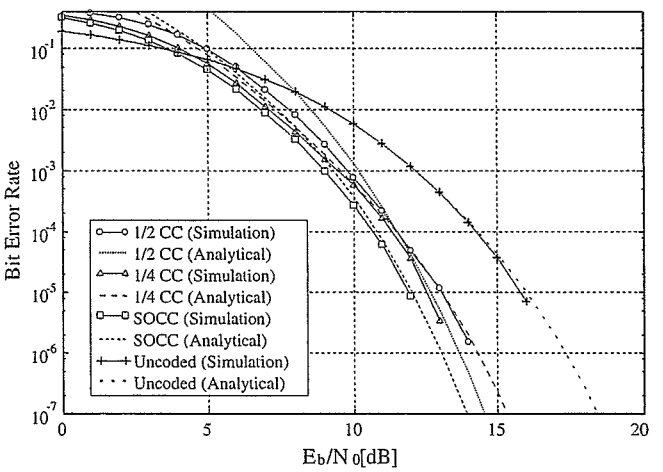

Figure 4. Comparison of BER for different convolutional coding schemes in terms of E_b/N_0 for MRC-RAKE receiver for $L = 8$, $N_u = 1$, $K = 5$, Channel Model=CM3.

4.2. Performance for Single-User ISI Channel

Figure 4 shows the BER versus SNR per information bit, E_b/N_0 , where E_b is the average received energy per information bit. The solid lines and the dotted lines represent the Monte–Carlo simulation results and the analytical upper bound of BER for MRC-RAKE receiver. In the Monte-Carlo simulation, 30, 000 bits are sent for each channel and BERs are averaged over 100 different multipath channels. In this figure, simulation results and analytical results are in good agreement for all schemes. In a single-user environment, the receiver suffers only from ISI. This figure shows that performance of SOCC does not deteriorate so much because of its strong error correction capability (or large free distance), though the performance depends on the total bandwidth expansion factor. Therefore, in this case, MMSE receiver is not necessary.

4.3. Performance for Multi-user Channel

Figures 5–8 show the BER versus E_b/N_0 for multipath and multiple access environment. Again, channel model is CM 3, and the number of users is 30. For simplicity, we assume that the received energies of all users are the same; i.e., $A_k = 1$ for all k. In our simulations, we

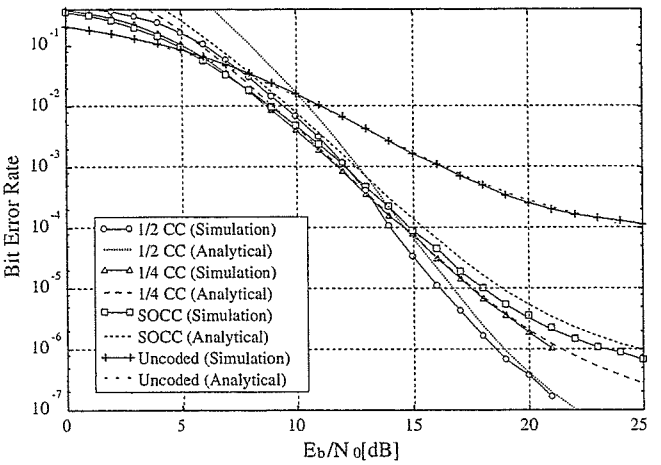

Figure 5. Comparison of BER for different convolutional coding schemes in terms of E_b/N_0 for MRC-RAKE receiver for $L = 8$, $N_u = 30$, $K = 5$, $J = 1$, Channel Model=CM3.

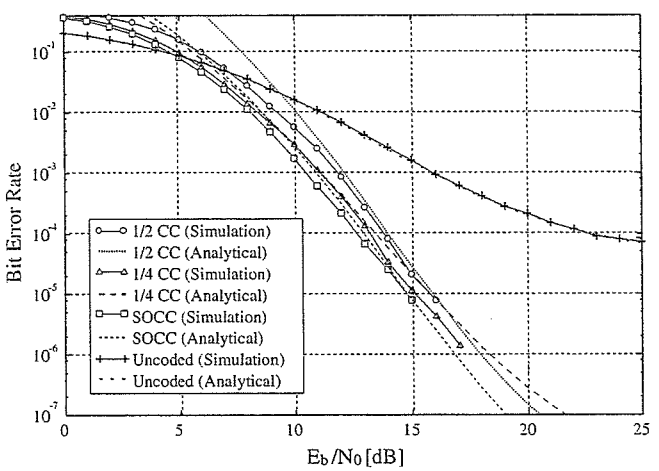

Figure 6. Comparison of BER for different convolutional coding schemes in terms of E_b/N_0 for MRC-RAKE receiver for $L = 8$, $N_u = 30$, $K = 5$, $J = 4$, Channel Model=CM3.

generate 100 channel impulse responses for the desired user in the same way as in the previous case. An additional assumptions are made that all users experience independent, but the same type of fading, that is, all users experience CM 3.

Figure 5 shows the performance of MRC-RAKE receiver using single spreading sequence ($J = 1$). This figure shows that the performance deteriorates gradually when the coding rate decreases (except the uncoded case). The reason for the performance degradation is that, in the system employing single spreading, the performance largely depends on the length of the spreading sequence because the interference coefficient remains unchanged during the transmission time. As a result, the variance of the interference terms increase.

Figure 6 shows the BER performance of MRC-RAKE receiver using CH scheme with $J = 4$. As opposed to the previous result, in Figure 6, the BER performance is improved as the coding rate decreases. This is due to the fact that by using multiple spreading sequence, the

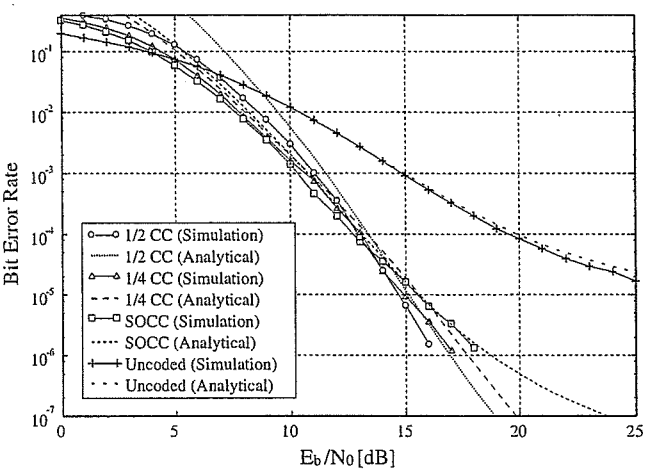

Figure 7. Comparison of BER for different convolutional coding schemes in terms of E_b/N_0 for MMSE-RAKE receiver for $L = 8$, $N_u = 30$, $K = 5$, $J = 1$, Channel Model=CM3.

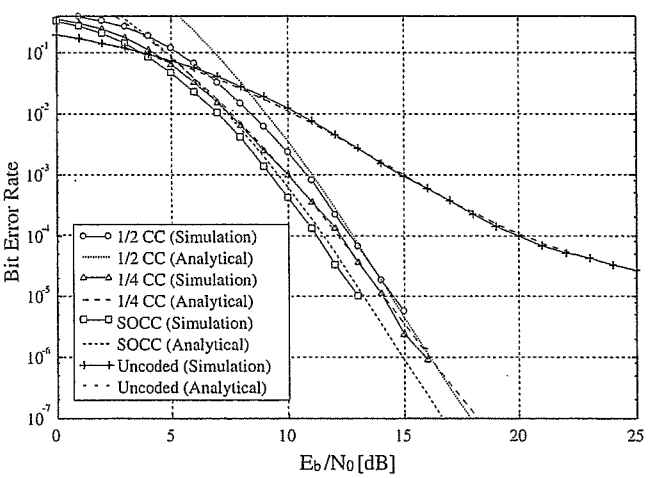

Figure 8. Comparison of BER for different convolutional coding schemes in terms of E_b/N_0 for MMSE-RAKE receiver for $L = 8$, $N_u = 30$, $K = 5$, $J = 4$, Channel Model=CM3.

interference coefficients change from symbol to symbol, which allows the interference terms to be treated as noise. In other words, MUI is closer to Gaussian distribution than that when single spreading sequence is employed.

Next, Figures 7 and 8 show the BER performance of MMSE-RAKE combining receiver for $J = 1$ (single spreading sequence) and $J = 4$ (CH). In contrast to the MRC combining scheme, in Figure 7, the BER performance does not deteriorate even in the case of $J = 1$, because the MMSE filter effectively suppresses the interference. Figures 9 and 10 show the theoretical upper bound of BER in terms of the active number of users. From these figures, we can find that the lower the coding rate is, the better the performance becomes. Moreover, the difference is bigger in Figure 9 than Figure 10. The performance of 1/2 CC is not improved even if MMSE receiver is employed.

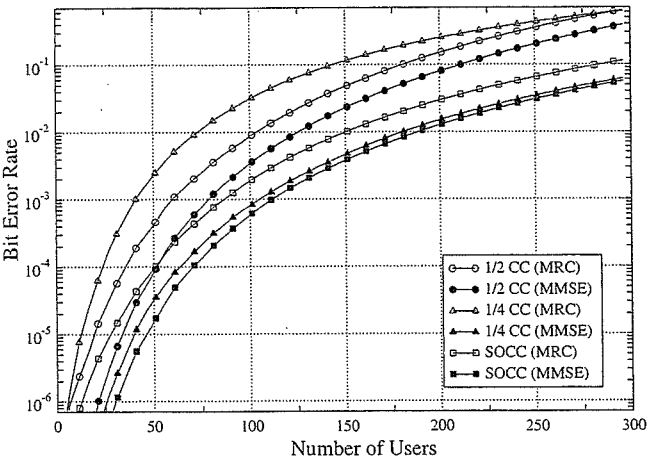

Figure 9. Comparison of BER for different convolutional coding schemes in terms of number of active users for both MRC-RAKE receiver and MMSE-RAKE receiver for $E_b/N_0 = 15$ [dB], $K = 5$, $L = 8$, Channel Model=CM3.

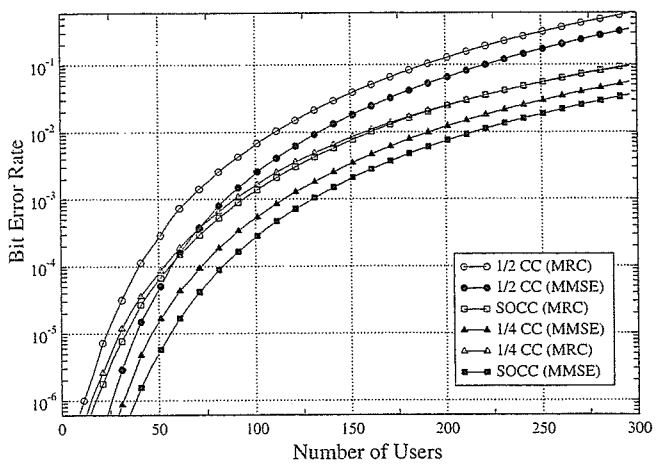

Figure 10. Comparison of BER for different convolutional coding schemes in terms of number of active users for both MRC-RAKE receiver and MMSE-RAKE receiver for $E_b/N_0 = 15$ [dB], $K = 6$, $L = 8$, Channel Model=CM3.

4.4. SPECTRAL EFFICIENCY

Finally, Figures 11 and 12 show the comparison of the achievable spectral efficiency in terms of the total spreading factor. Here the spectral efficiency is defined as $N_u R_b$, where N_u denotes the maximum number of users to achieve a certain performance. A target BER, $P_b < 10^{-4}$, is assumed. It can be found that the lower the coding rate is, the bigger the achievable system capacity becomes. In addition to this, MMSE receiver effectively suppresses the interference from other users and further increases the system capacity.

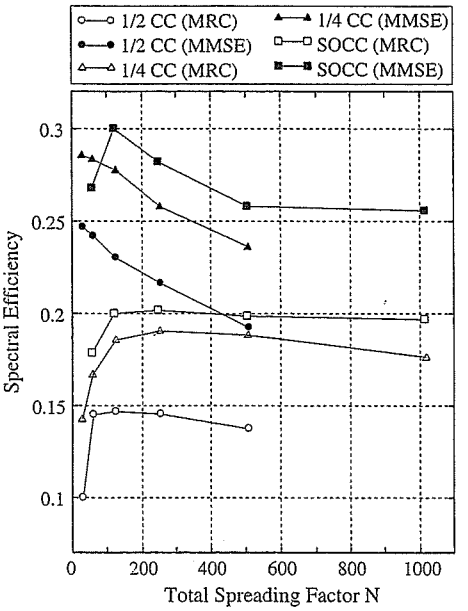

Figure 11. Achievable spectral efficiency in terms of total spreading factor for $E_b/N_0 = 15$[dB], BER=10^{-4}, $L = 8$, $J = 4$, $K = 5$, Channel Model=CM3.

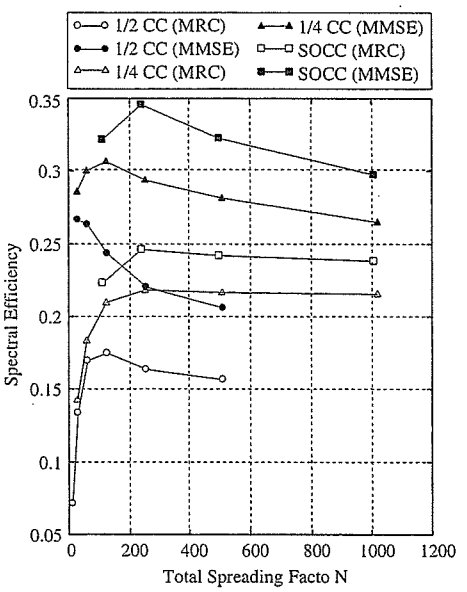

Figure 12. Achievable spectral efficiency in terms of total spreading factor for $E_b/N_0 = 15$[dB], BER=10^{-4}, $L = 8$, $J = 4$, $K = 6$, Channel Model=CM3.

5. Conclusions

In this paper, the use of SOCC to improve the average BER performance of DS-UWB systems over multipath and multiple access environment was studied. Analysis of the effect of MUI and ISI on the BER performance of SOCC assuming two types of receiver, MRC-RAKE

receiver and MMSE-RAKE receiver, was performed. Our analysis showed that in the case of employing simple MRC-RAKE receiver, the BER performance of SOCC was affected by MUI and ISI because of the short length of spreading sequence.

In order to combat MUI and ISI, first CH scheme was employed in conjunction with SOCC to make the interference independent from symbol to symbol. The results showed that SO coded scheme outperforms the higher-rate conventional convolutional coded scheme for multipath and multiple access channels when it is combined with CH. Analysis of MMSE-RAKE receiver to suppress interferences, was also performed. The BER performance of SOCC using MMSE-RAKE receiver was better than the one of higher-rate codes even if short-spreading codes were used. In the case of MMSE receiver, the use of CH improved the BER performance.

A conclusion that can be drawn is that, for UWB systems, low-rate channel code is effective if it is combined with CH or some interference suppression strategy like MMSE filtering. Also, it can be concluded that for low-data rate and low-cost applications, such as low-rate WPAN, combined low-rate coding and scrambling, or CH is suitable. For high-rate WPAN using relatively large number of RAKE fingers, combined SOCC and MMSE-RAKE receiver is effectively increase the system capacity.

References

1. A. J. Viterbi, *CDMA : Principles of Spread Spectrum Communication*. Addison Wesley, 1995.
2. A. J. Viterbi, "Very Low Rate Convolution Codes for Maximum Theoretical Performance of Spread-Spectrum Multiple-Access Channels," *IEEE Journal on Selected Areas in Commun.*, Vol. 8, No. 4, pp. 641–649, 1990.
3. P. D. Shaft, "Low-Rate Convolutional Code Applications in Spread-Spectrum communications," *IEEE Transactions on Communications*, Vol. 25, No. 8, pp. 815–822, 1977.
4. P. Frenger, P. Orten, and T. Ottosson, "Code-Spread CDMA Using Maximum Free Distance Low-Rate Convolutional Codes," *IEEE Transactons on Communication*, Vol. 48, No. 1, pp. 135–144, 2000.
5. M. L. Welborn, "System Considerations for Ultra-Wideband Wireless Networks," *Proceedings of the IEEE Radio and Wireless Conf.*, Boston, MA, Aug. 19–22, 2001.
6. A. R. Fourouzan, M. Nasiri-Kenari, and J. A. Salehi, "Performance Analysis of Time-Hopping Spread-Spectrum Multiple-Access Systems: Uncoded and Coded Schemes", *IEEE Trasactions on Communications*, Vol.1, No. 4, pp. 671–681, 2002.
7. A. R. Fourouzan, M. Nasiri-Kenari, and J. A. Salehi, "Low-Rate Convolutionally Encoded Time-Hopping Spread Spectrum Multiple Access Systems", *Proceedings of the IEEE International Symposium on Personal, Indoor and Mobile Radio Communications*, Barcelona, Spain vol. 2, pp. 1555–1558, 2000.
8. J. Foerster, Channel Modeling Sub-committee Report Final, IEEE P802.15 Working Group for Wireless Personal Area Networks (WPANs), IEEE p802.15 02/49orl SG3a, Feb 2002.
9. N. Yamamoto, "Performance Evaluation of internally Low Rate Turbo Coded UWB-IR Systems", *IEICE technical report*, Microwaves, pp. 135–140, 2003.
10. K. Tang, P. H. Siegel, and L. B. Milstein, "A Comparison of Long versus Short Spreading Sequences in Coded Asynchronous DS-CDMA Systems," *IEEE Journal on Selected Areas in Communication*, Vol. 19, pp. 1614–1624, 2001.
11. J. D. Choi, "Performance of Ultra-Wideband Communications With Suboptimal Receivers in Multipath Channels," *IEEE Journal of Selected Areas Communication*, Vol. 20, No. 9, pp. 1754–1766, 2002.
12. J. G. Proakis, *Digital Communications*. Mcgraw-Hill, 1995.

Tomoko Matsumoto was born in Ehime, Japan, in 1981. She received the M.S. degree in Division of Physics, Electrical and Computer Engineering from Yokohama National University, Yokohama, Japan, in 2005. She is currently working toward the Ph.D. degree in electrical and computer engineering at Yokohama National University, Yokohama, Japan. Her research interests include ultra-wideband communications, channel coding in wireless communications and information theory. She is a student member of the IEICE and IEEE.

Ryuji Kohno received the Ph.D. degree from the University of Tokyo in 1984. Dr. Kohno is currently a Professor of the Division of Physics, Electrical, and Computer Engineering, Yokohama National University. In his career, he was a director of Advanced Telecommunications Laboratory of SONY CSL during 1998–2002 and currently a director of UWB Technology institute of National Institute of Information and Communications Technology (NICT). In his academic activities, he was elected as a member of the Board of Governors of IEEE Information Theory (IT) Society in 2000 and 2003. He has played a role of an editor of the IEEE Transactions on IT, Communications, and Intelligent Transport Systems (ITS). He is a fellow of IEICE, vice-president of Engineering Sciences Society of IEICE and has been the Chairman of the IEICE Technical Committee on Spread Spectrum Technology, that on ITS, and that on Software Defined Radio (SDR). Prof. Kohno has contributed for organizing many international conferences, such as an chair-in honor of 2002 & 2003 International Conference of SDR (SDR'02 & SDR'03), a TPC co-chair of 2003 International Workshop on UWB Systems(IWUWBS'03), and a general co-chair of 2003 IEEE International Symposium on IT (ISIT'03), that of Joint UWBST&IWUWB'04 and IWUWBT'05, and so on. He was awarded IEICE Greatest Contribution Award and NTT DoCoMo Mobile Science Award in 1999 and 2002, respectively.

IEICE TRANS. FUNDAMENTALS, VOL.E89–A, NO.11 NOVEMBER 2006

PAPER Special Section on Wide Band Systems

Interference Reduction Using a Novel Pulse Set for UWB-CDMA Systems

Hiroki HARADA[†a)], *Student Member and* Ryuji KOHNO[†b)], *Fellow*

SUMMARY A novel UWB system for a new indoor short distance radio-communication is examined. Various types of UWB systems have been proposed in the literature. Particularly direct sequence (DS) systems and time hopping (TH) systems are attractive due to low power consumption and a simple transceiver construction. In this paper, we consider to apply *modulated and modified Hermite pulses* (MMHP) for both DS-UWB and TH-UWB systems. Furthermore, MMHP are extended to a novel pulse set referred as *limited bandwidth MMHP set* in order to reduce various interferences. It is composed of pseudo-orthogonal pulses that have both good auto-correlation characteristics in all orders and low cross-correlation characteristics between different orders. The proposed pulse set also have some specific notches, which can be used to reduce narrow-band interference (NBI). Additionally, we propose a novel pulse shape hopping that employs the proposed MMHP set. Multi-user interference (MUI) and inter-symbol interference (ISI) can be reduced by such a pulse shape hopping scheme for the DS or TH UWB signal format. Simulation results show significant performance improvements by using the proposed UWB system.

key words: *UWB-WPAN, modulated and modified Hermite pulse (MMHP), pulse shape hopping, asynchronous communication, interference reduction*

1. Introduction

Ultra wideband (UWB) communications occupy a very wide transmission bandwidth as its name suggests. More specifically, such a bandwidth has to exceed 500 MHz or 20% of its center frequency. The frequency range is typically in the order of one to several GHz. While UWB communications can achieve high data rate transmission with low complexity, it can provide robustness against various distortions such as multipath fading as well. Hence, UWB wireless communication systems has raised enormous interest in the area of short distance wireless communications [1]. UWB systems have been studied actively since the Federal Communications Commission (FCC) of USA authorized the civil use of UWB signals in February 2002. In such regulation, UWB communication systems have to fullfill a spectral mask that limits the maximum transmission power in order to co-exist with other narrowband and wideband wireless communication systems already operating in the approved spectrum. Indeed, the FCC provides with spectral masks that regulate UWB transmission in the frequency band from 3.1 GHz to 10.6 GHz.

Manuscript received March 3, 2006.
Manuscript revised May 21, 2006.
Final manuscript received July 13, 2006.

[†]The authors are with the Division of Electrical and Computer Engineering, Faculty of Engineering, Yokohama National University, Yokohama-shi, 240-8501 Japan.
a) E-mail: hhiroki@ieee.org
b) E-mail: kohno@ynu.ac.jp

DOI: 10.1093/ietfec/e89–a.11.3050

Originally, UWB communication systems was proposed as impulse radio (IR) UWB, which is based on the transmission of baseband pulses. However, different types of UWB systems based on conventional carrier-based communications have been proposed as well. For instance, multi-band OFDM and DS-UWB systems consider the use of set of carriers and a carrier signal, respectively [2]–[4]. UWB systems that introduce such conventional technologies are effective in terms of feasibility [5]. However, such systems lose some advantages, e.g., low power consumption and simple circuitry.

In multiple access schemes using DS or TH, a pulse position modulation (PPM), a bi-phase modulation and a pulse shape modulation have been proposed [6]–[8]. Additionally, as a transmitting waveform, a monocycle waveform and some orthogonal pulses have also been proposed [9], [10]. Modified Hermite pulses are generated by Hermite polynomials that are modified to become orthogonal [11]. An orthogonal pulse modulation (OPM) is proposed in [12]. The OPM is effective in the case of synchronous communications. However, OPM loses the orthogonality property in the case of asynchronous communications [13].

The performance degradation in terms of bit error probability is mainly caused by three factors [2]. The first is multi-user interference (MUI) from other users in the system. The second is inter-symbol interference (ISI), which is caused by frequency selective channels. The third is co-channel interference such as narrow band interference (NBI), which is the interference from co-existing narrowband and wideband communication systems. For instance, 5 GHz WLAN systems. In UWB-WPAN systems, it is required that the system reduces these interferences effectively.

In this paper, we examine the UWB communication system that uses *modulated and modified Hermite pulses* (MMHP). The MMHP are modulated pulses based on modified Hermite polynomials (MHP). In addition, we design a novel pulse set that occupy the same bandwidth for all orders in order to satisfy the FCC spectral mask effectively. Our proposed MMHP pulse set is denominated as *limited bandwidth MMHP set*. It is composed of pseudo-orthogonal pulses of different order with good correlation characteristics. That is, the cross-correlation values of the proposed MMHP are low, and additionally the spectrum of the MMHP has notches, whose number is the same as the MMHP order. In the proposed system, users use MMHP of different orders at the same time in combination with either

DS or TH so that the effect of MUI can be reduced.

Furthermore, our proposed system can resolve the problem of co-existence between UWB systems and other systems. For instance, the WLAN system "IEEE802.11a," which is allocated around 5 GHz [14]. We use notches of the proposed MMHP to reduce the overlap between the spectrum of the proposed UWB system and the spectrum of the WLAN system so that NBI is reduced effectively.

In the literature [3], [15], [16], several proposals to deal with interferences can be found. However, those solutions introduce more complexity to the system. Alternatively, we develop the novel pulse set as well as the innovative method of pulse shape hopping, which outperforms conventional systems in terms of interference suppression. Additionally, by using the novel pulse set together with pulse shape hopping scheme, the proposed system keeps also the advantage of low transceiver complexity.

The rest of the paper is organized as follows. The conventional DS-UWB and TH-UWB systems are described in Sect. 2. In Sect. 3, we outline our proposed UWB system using the limited bandwidth MMHP set. In Sect. 4, numerical comparison between the proposed system and the conventional UWB system is presented. Finally, conclusions and future work are remarked in Sect. 5.

2. TH-UWB and DS-UWB System Model

In this section we revise briefly the conventional TH-UWB system [1] and DS-UWB system [2], [3]. We consider the TH-UWB system and the DS-UWB system as a benchmark for our proposed system, since TH-UWB and DS-UWB systems have simple circuitry and low power consumption.

Normally, two types of data modulation are considered for TH-UWB systems, binary antipodal modulation and binary PPM. The binary antipodal modulation scheme outperforms binary PPM scheme in terms of bit error probability. Moreover, polarity reversals can eliminate the spectral lines and reduce the peak-to-average ratio. Thus, the binary antipodal modulation scheme is used as a data modulation scheme in our proposed system throughout the paper. However our results can be readily extended to binary PPM.

2.1 TH-UWB System Model

TH-UWB impulse radio is built upon position shift of pulses with a certain shape in the time domain. A system with TH-UWB can accommodate multiple simultaneous users by assigning an appropriate hopping sequence to each user in asynchronous communications. In TH-UWB, the transmitted signal from the k-th transmitter using binary antipodal modulation can be defined as

$$s_t^{(k)}(t) = \sum_{i=0}^{\infty} b^{(k,i)} \sum_{j=0}^{N_s-1} w_{tr}(t - jT_f - c_t^{(k,j)}T_c - iT_b), \quad (1)$$

where $w_{tr}(t)$ is the transmission pulse shape, and $b^{(k,i)} \in \{\pm 1\}$ is a binary information bit sequence for the k-th user. $w_{tr}(t-jT_f-c_t^{(k,j)}T_c-iT_b)$ indicates the j-th pulse transmitted by the k-th user at $t = jT_f + c_t^{(k,j)}T_c + iT_b$. The pseudorandom time-hopping sequence for the k-th user is given by $[c_t^{(k,0)}, c_t^{(k,1)}, \ldots, c_t^{(k,N_s-1)}]^T$, where $c_t^{(k,j)} \in [0, N_h]$. T_c is the chip duration and T_f is the frame duration, which is greater than or equal to N_hT_c. The information bit duration is represented by T_b. The number of hops in each bit duration is designated by N_s, and T_b equals N_s times frame duration T_f, i.e., $T_b = N_sT_f$.

2.2 DS-UWB System Model

DS-UWB system employs transmission pulses that are spreaded by pseudorandom sequences in the chip level. Since different sequences are assigned to users, DS-UWB system can accommodate multiple simultaneous users as well as TH-UWB system. In DS-UWB, the transmitted signal from the k-th transmitter using binary antipodal modulation can be defined as

$$s_d^{(k)}(t) = \sum_{i=0}^{\infty} b^{(k,i)} \sum_{j=0}^{N_s-1} c_d^{(k,j)} \cdot w_{tr}(t - jT_c - iT_b), \quad (2)$$

where the information bit duration is represented by $T_b = N_sT_c$. The pseudorandom spreading sequence for k-th user is given by $[c_d^{(k,0)}, c_d^{(k,1)}, \ldots, c_d^{(k,N_s-1)}]^T$, where $c_d^{(k,j)} \in \{\pm 1\}$. It is known that DS-UWB outperforms TH-UWB when the number of users is lower than the spreading factor N_s [17]. On the contrary, when MUI is dominant, both DS and TH systems exhibit similar performance.

2.3 Received Signal Representation

If there are N_u active users in the system, the composite received signal at the output of the receiver antenna is given by

$$r(t) = \sum_{k=0}^{N_u-1} h^{(k)}(t) \otimes s^{(k)}(t) + \nu(t), \quad (3)$$

where $h^{(k)}(t)$ is the k-th UWB channel impulse responce, $s^{(k)}(t)$ represents the received signal from the k-th transmitter, and $\nu(t)$ represents composite noises that include NBI and the thermal noise. Without loss of generality, we assume that user $k = k'$ is the detection target. Therefore, (3) can be rewritten as

$$r(t) = h^{(k')}(t) \otimes s^{(k')}(t) + \sum_{k \neq k'}^{N_u-1} h^{(k)}(t) \otimes s^{(k)}(t) + \nu_n(t) + \nu_a(t), \quad (4)$$

where $\nu_n(t)$ is NBI and $\nu_a(t)$ is additive white Gaussian noise (AWGN). In (4), the first term represents target signal including ISI. On the other hand, the second term of (3) represents MUI.

UWB channels have a large delay spread. Thus, UWB

communications suffer from ISI severely. We here employ the IEEE802.15.3a channel model as the UWB multipath fading channel model throughout the paper [18].

Originally, IR-UWB systems employing short baseband pulses, those were implemented by exciting a conventional monopole antenna with a stepped in amplitude method, whose output can be modeled mathematically as the first derivative of a gaussian pulse [1]. So, it had been assumed that the transmitted UWB pulse shape is distorted by transmit and receive antennas [19]. However, novel UWB antenna designs do not introduce waveform distortions such as derivative effects [20].

3. Proposed UWB System Using Novel Pulse Set

In this section we explain our proposed UWB system using the MMHP.

3.1 Pulse Set Design (Limited Bandwidth)

A given user sends pulses in a certain timing pattern with an unique DS or TH sequence. In our proposed system, users utilize modified MMHP waveforms of various orders, in contrast to the case of single pulse waveform in conventional DS-UWB and TH-UWB systems. The MMHP and their characteristics are described below.

Hermite polynomials are modified to become orthogonal and are represented as follows [11]

$$g^{(n)}(t) = e^{-\frac{t^2}{4}} h_e^{(n)}(t) = (-1)^n e^{\frac{t^2}{4}} \frac{d^n}{dt^n}\left(e^{-\frac{t^2}{2}}\right), \quad (5)$$

where $h_e^{(n)}(t)$ is Hermite polynomial and n is the order of this MHP. Thus, MHP functions with different order are orthogonal to each other when they are perfectly aligned. However, the FCC spectral mask regulates the use frequencies from 3.1 GHz to 10.6 GHz. Unfortunately, MHP pulses do not fulfill this spectral mask [21]. Thus, the MHP pulses are modulated by a carrier signal of frequency f_c represented as

$$\begin{aligned} g_m^{(n)}(t) &= g^{(n)}(t)\cos(2\pi f_c t) \\ &= (-1)^n \cos(2\pi f_c t) e^{\frac{t^2}{4}} \frac{d^n}{dt^n}\left(e^{-\frac{t^2}{2}}\right). \end{aligned} \quad (6)$$

Equation (6) is denominated as MMHP waveform. Figures 1 and 2 show the time and frequency domain representations of the MMHP for $f_c = 6.85$ GHz, and orders $n = 0, 1, 2, 3, 4$.

The MMHP can fulfill the FCC spectral mask. Additionally, the MMHP are efficient waveforms since the MMHP can be generated by an oscillator and the simple MHP generator [12].

However, the bandwidth of the MMHP extends as the order increases. Therefore, the MMHP of higher order cannot be used in the case of fulfilling the FCC spectral mask [21]. Moreover, different orders of the MMHP have different bandwidth respectively. Since, robustness against multipath fading varies with the order of the transmitted MMHP.

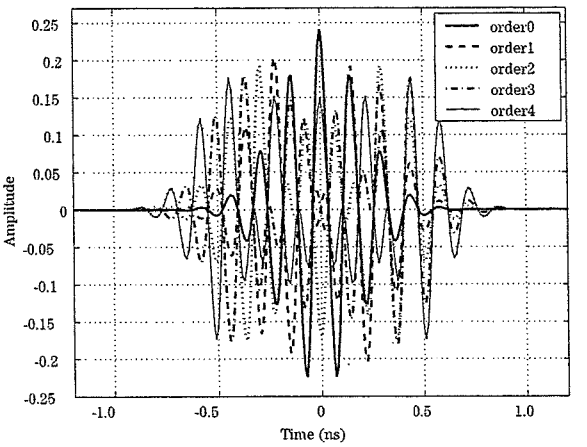

Fig. 1 The time domain representation of the MMHP: order 0, 1, 2, 3, 4.

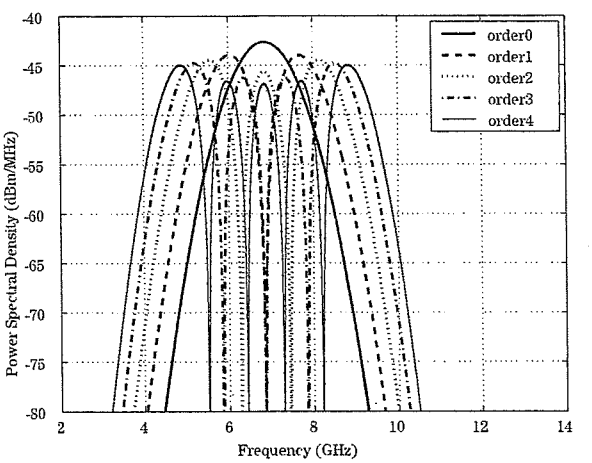

Fig. 2 The frequency domain representation of the MMHP: order 0, 1, 2, 3, 4.

So, we improve the waveforms to resolve these problems. Equation (6) can be transformed as follows

$$\begin{aligned} g_{LB}^{(n)}(t) = N^{(n)}(-1)^n \cos(2\pi f_c t) \exp\left[\frac{\left(\frac{t}{t_p}\right)^2}{4}\right] \\ \cdot \frac{d^n}{dt^n}\left(\exp\left[-\frac{\left(\frac{t}{t_p}\right)^2}{2}\right]\right). \end{aligned} \quad (7)$$

$N^{(n)}$ is a normalizing parameter and t_p is a parameter which controls the pulse width. If t_p increases, the bandwidth of the pulse becomes narrower. Table 1 shows the pulse width and the limit of the enabled orders when the bandwidth fits into the 3.1 GHz to 10.6 GHz band. The value of t_p is fixed properly for each order so that the MMHP of different orders have the same bandwidth. Consequently, even if the MMHP of higher order are used, the bandwidth can be fit into the bounds of the spectral mask as shown in Fig. 3, where the

Table 1 The suitable values of pulse width parameters and the orders for a 3.1 GHz to 10.6 GHz bandwidth.

order n	pulse width parameter t_p (nsec)
0	0.0375
1	0.0625
2	0.0781
3	0.0906
4	0.1031
5	0.1125
6	0.1219
7	0.1313
8	0.1375

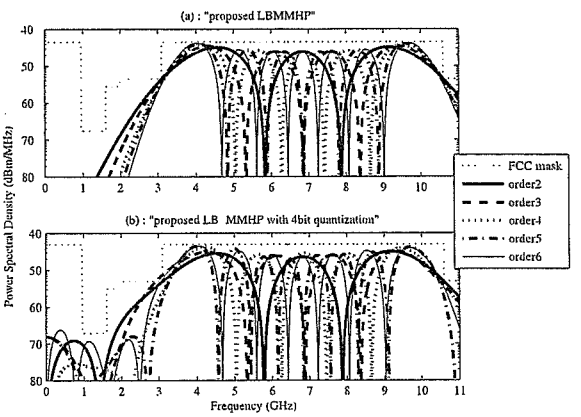

Fig. 3 The frequency domain representation of the limited bandwidth MMHP set: order 2, 3, 4, 5, 6.

sampling frequency is 25 GHz. The proposed pulse set is denominated as *limited bandwidth MMHP (LB-MMHP) set.*

The novel set of LB-MMHP that is generated in this way has the following characteristics:

- LB-MMHP with different order are pseudo-orthogonal to each other when they are perfectly aligned.
- LB-MMHP waveforms have sharp auto-correlation characteristics in all orders in contrast to the conventional set of MMHP waveforms.
- The cross-correlation between different orders is low and independent of the time lag.
- The spectrum of each LB-MMHP of different order has notches whose number is the same as its order.

3.2 Correlation Characteristics Analysis

As follows, we confirm correlation characteristics of the LB-MMHP set.

The correlation value of the proposed LB-MMHP $C^{(m,n)}(\tau)$ is given by

$$C^{(m,n)}(\tau) = \int_{-\infty}^{\infty} g_{LB}^{(m)}(t) \cdot g_{LB}^{(n)}(t-\tau)dt. \quad (8)$$

Table 2 shows the correlation values of the proposed LB-MMHP in the case of $\tau = 0$. This table indicates that the orthogonality is lost when the bandwidth of all orders fits into the spectral mask. However, the correlation values are

Table 2 Correlation values $C_{m,n}(0)$ of the proposed LB-MMHP for a 3.1 GHz to 10.6 GHz bandwidth.

m, n	0	1	2	3	4	5	6	7	8
0	1	0	−0.4	0	0.3	0	−0.2	0	0.2
1	-	1	0	−0.4	0	0.3	0	−0.3	0
2	-	-	1	0	−0.4	0	0.3	0	−0.3
3	-	-	-	1	0	−0.4	0	0.3	0
4	-	-	-	-	1	0	−0.4	0	0.3
5	-	-	-	-	-	1	0	−0.4	0
6	-	-	-	-	-	-	1	0	−0.4
7	-	-	-	-	-	-	-	1	0
8	-	-	-	-	-	-	-	-	1

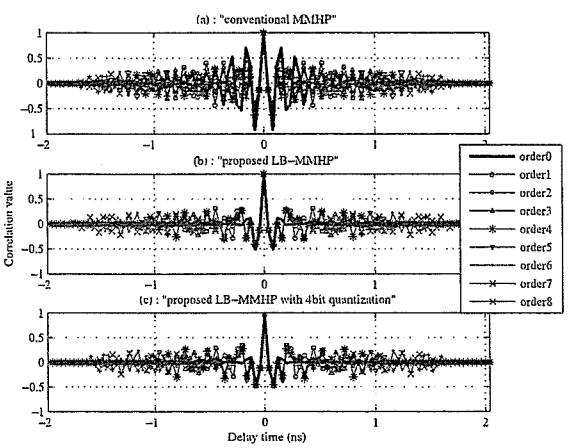

Fig. 4 An auto-correlation characteristic of both conventional MMHP, proposed LB-MMHP and LB-MMHP with 4 bit quantization levels of order ranging from 0 to 8.

zero in the cases of both $m + n = 2i + 1$ $(i = 0, 1, 2, ...)$ and $m \neq n$. Additionally, the correlation values are low in the cases of both $m + n = 2i$ and $m \neq n$. So, we can consider the LB-MMHP as a pseudo-orthogonal pulse set.

Figure 4 shows the auto-correlation characteristic of both the conventional MMHP, the LB-MMHP and the LB-MMHP with 4 bit quantization levels based on Eq. (8). Auto-correlations of proposed LB-MMHP of all orders have the same peaks and low auto-correlation values around time lag 0, as contrasted to the conventional MMHP. This improvement of correlation is caused by changing the pulse durations of MMHP.

On the other hand, Fig. 5 shows the cross-correlation characteristics of both the conventional MMHP, the LB-MMHP and the LB-MMHP with 4 bit quantization levels based on Eq. (8). We can see that the cross-correlation between different orders is lower than the auto-correlation and independent of the time lag in the cases of both conventional MMHP and proposed LB-MMHP.

Furthermore, by Figs. 4 and 5, we can see that the 4 bit quantization levels are enough for proposed pulses to keep their correlation characteristics. Since less than 4 bit quantization levels will cause performance degradation of correlation characteristics, so these waveforms need over 4 bit quantization levels. Additionally, power spectral densities of quantized waveforms are shown as Fig. 3(b). Al-

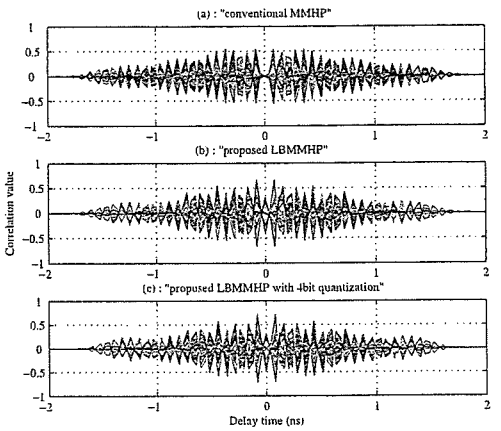

Fig. 5 A cross-correlation characteristic of both conventional MMHP, proposed LB-MMHP and LB-MMHP with 4 bit quantization levels of all combinations of orders ranging from 0 to 8.

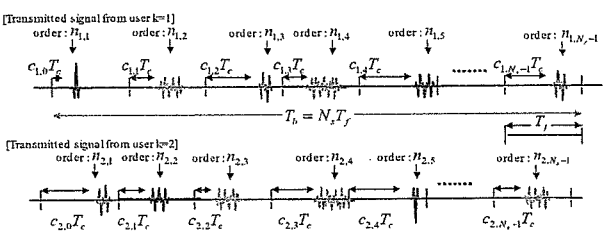

Fig. 6 Transmitted signals from user $k = 1$ and user $k = 2$ in our proposed TH system using the LB-MMHP set and pulse shape hopping.

though they are different from original power spectral densities, they can fulfill FCC indoor spectral mask except for orders 0 and 1.

3.3 Pulse Shape Hopping Using the LB-MMHP Set

As a way of reducing effects of ISI and MUI, we propose the pulse shape hopping using LB-MMHP.

In the proposed scheme with TH, a user employs LB-MMHP of different orders following a time hopping sequence as illustrated in Fig. 6. Thus, a user sends the LB-MMHP waveform whose order is decided by a unique pseudo-random noise (PN) sequence to hop the order, in exact timing with an unique time hopping (TH) sequence. The k-th user's transmitted signal $s_{TH}^{(k)}(t)$ is given by

$$s_{TH}^{(k)}(t) = \sum_{i=0}^{\infty} b^{(k,i)} \sum_{j=0}^{N_s-1} g_{LB}^{(n_{k,i,j})}(t - jT_f - c_t^{(k,j)}T_c - iT_b), \tag{9}$$

where the sequence set elements $n_{k,i,j}$ is a pseudorandom pulse shape hopping sequence for the k-th user, whose range is between the minimum hopping order of the LB-MMHP n_{min} and the maximum hopping order of the LB-MMHP n_{max}.

Additionally, the proposed scheme can be also applied to DS-UWB systems as well. In the proposed scheme with

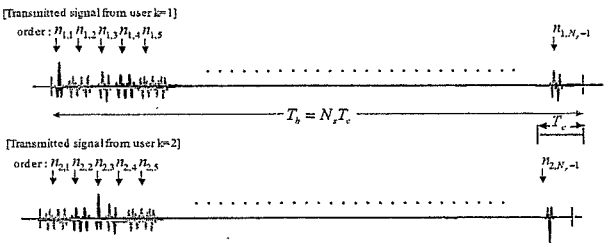

Fig. 7 Transmitted signals from user $k = 1$ and user $k = 2$ in our proposed DS system using the LB-MMHP set and pulse shape hopping.

DS, the k-th user's transmitted signal $s_{DS}^{(k)}(t)$ is given by

$$s_{DS}^{(k)}(t) = \sum_{i=0}^{\infty} b^{(k,i)} \sum_{j=0}^{N_s-1} c_d^{(k,j)} \cdot g_{LB}^{(n_{k,i,j})}(t - jT_c - iT_b), \tag{10}$$

as illustrated in Fig. 7.

We assume that the receiver has knowledge of both the time-hopping sequence and the pulse shape hopping sequence of the desired user. Additionally, perfect synchronization is assumed. A correlator in the receiver measures the correlation values between the received signal $r(t)$ and a template signal $v(t)$. Data are demodulated by the correlation detection. This operation is represented by

$$CP^{(k,i)} = \int_{iT_b}^{(i+1)T_b} r(t) \cdot v^{(k)}(t - iT_b)dt, \tag{11}$$

$$\hat{b}^{(k,i)} = sgn(CP^{(k,i)}), \tag{12}$$

where CP is the output of the correlator, $\hat{b}^{(k,i)}$ is the decision statistic of the coherent detection, and the template signal $v(t)$ is given by

$$v^{(k)}(t) = \begin{cases} \sum_{j=0}^{N_s-1} c_d^{(k,j)} \cdot g_{LB}^{(n_{k,i,j})}(t - jT_c) \\ \text{for DS,} \\ \sum_{j=0}^{N_s-1} g_{LB}^{(n_{k,i,j})}(t - jT_f - c_t^{(k,j)}T_c) \\ \text{for TH.} \end{cases} \tag{13}$$

The received signal $r(t)$ includes not only the desired signal $s^{(k)}(t)$, but also the interference signal from other users, ISI, and all other kinds of noise sources.

As it is described in Sect. 1, the ISI is caused by the effect of multi-path fading. Delayed pulses of a signal interfere with next pulses in particular the case of a high data rate communication. The level of ISI is decided by the channel's delay spread and the auto-correlation function of the transmitted signal.

For asynchronous communication, the correlation output of the MUI component is given by

$$MUI = \int_0^{N_s \cdot T_f} \left[\sum_{k \neq k'}^{N_u} h^{(k)}(t) \otimes s^{(k)}(t - \tau_k) \right] \cdot v(t)dt, \tag{14}$$

where $s^{(k)}(t)$ is the transmitted signal of k-th user, τ_k is a random delay time, and N_u is the number of users in the system. The value of MUI is decided by the cross-correlation function between other user's signals $k \neq k'$ and the template signal for desired user k'.

Therefore, MUI can be reduced if users use different pulses that have low cross-correlation characteristics each other simultaneously. The cross-correlation between the proposed LB-MMHP of different orders is low and independent of the time lag as it is described in Sect. 3.2. So, the proposed system employs a Reed-Solomon (RS) sequences as the pulse shape hopping sequences for users in order to keep the number of waveforms as few as possible. For instance, a RS sequence is used to select the MMHP that forms a user signature waveform, such that a given MMHP is just repeated 1 time for another user's signature waveform at the same chip time.

The MMHP generator of our proposed system needs a MHP generator and only one oscillator. Additionally, the MHP of higher order is generated by the MHP of low order and derivative circuits [11], [12]. However, generating the proposed pulses by analog circuitry requires high-precision devices such as delay lines that can make a long delay, high-precision variable attenuator, and so on. So, it is difficult for current technologies to generate such complex waveforms by analog circuitry. On the other hand, LB-MMHP can be synthesized with digital technology relatively easy. Although it requires very fast digital to analog converters (DACs), the advances on high speed electronics will make available the required DACs with a reasonable cost. Additionally, Figs. 4 and 5 indicate that a DAC with 4 bit quantization might be enough for our proposed pulses to maintain correlation characteristics. Since pulses occupy the frequency band from 3.1 GHz to 10.6 GHz, the DAC should have over 15 GHz sampling frequency. Because such DAC increases the cost significantly, alternatively, there is a scheme which can reduce the cost by using several parallel DAC of low sampling frequency instead of the DAC with high sampling frequency [22]. Consequently, we consider that it is possible to generate our proposed pulses with reasonable cost and high-precision. As compared with conventional UWB systems for WPAN, our system does not have complex circuitry including FFT such as multiband OFDM, and requires shorter spreading sequences for multiple access than spreading sequences of DS-UWB. So also in terms of hardware feasibility, our proposed system can countervail conventional systems.

4. Performance Evaluation

In this section we describe the result of performance evaluation.

4.1 Simulation Model

We consider the indoor short-distance multipath fading channel as the UWB communication environment and use the IEEE802.15.3a channel model [18]. Additionally, since DS-UWB is more practical than TH-UWB for WPAN, we use the conventional DS-UWB system and the proposed system combined with DS in our simulations.

Table 3 Parameters of the simulations.

channel model	CM1,2,3,4
number of transmitted bits	10^5
bandwidth	3.1–10.6 (GHz)
used LB-MMHP order	2–9
number of users	1,4,8,16
data modulation	bi-phase modulation
chip duration	2.6 (nsec)
time duration of 1 bit	2.6–49.4 (nsec)
number of pulse repetitions N_s	1–19
datarate	20.2–384.6 (Mbps)
receiver	Selective RAKE
number of fingers	1–50
combining	MRC
E_b/N_0	0–18 (dB)
SIR	−20–−4 (dB)

We assume an asynchronous communication system. In order to make simulations simple, the following assumptions are made:

- The transmitting pulses are quantized by 4 bit quantization levels, and there are no quantization in the receiver.
- The desired signal and the template signal are perfectly synchronized.
- Simulations do not include error correcting codes.
- The receiver knows both the DS sequence and the pulse shape hopping sequence used by the desired user.
- A Gold sequence is applied as the DS sequence in both our proposed system and a conventional DS-UWB system.
- A RS sequence is applied as the pulse shape hopping sequence in our proposed system.
- Signal to Interference Ratio (SIR) is defined as

$$SIR = \frac{\int_0^{T_b} |s^{(k)}(t)|^2 dt}{\sum_{k' \neq k}^{N_u} \int_0^{T_b} |s^{(k')}(t)|^2 dt}. \quad (15)$$

We use the 6-th derivative of Gaussian pulse in the conventional DS-UWB system for comparison. The bandwidth of this pulse can fulfill the FCC spectral mask. Parameters of the simulations are shown in Table 3.

4.2 Results

Figure 8 illustrates the BER performance for CM1 channels with $N_u = 1, 4, 8, 16$ users. In this figure, the proposed UWB system with DS as shown by Eq. (10) are compared to the conventional DS-UWB system using the 6-th derivative of a Gaussian pulse. Notice that our proposal offers better performance than the BER performance of the conventional system, specially in the case of multiple access. So, the pulse shape hopping scheme using LB-MMHP waveforms can reduce the effects of MUI and ISI since our proposal offers transmitted signals that have both good auto-